ADVANCED FUNCTIONAL MATERIALS
www.afm-journal.de

Enhancement of the Li Conductivity in LiF by Introducing Glass/Crystal Interfaces

Chilin Li, Lin Gu, and Joachim Maier*

For a variety of purposes, solid electrolytes with high ionic conductivity are believed to be an alternative to widely used liquid electrolytes. Most of them are developed based on the exploration of crystalline or amorphous structures. As a very rare example of the beneficial influence of glass/ceramic interfaces, we report the conductivity of LiF films on SiO_2. The LiF thin films are surprisingly found to be structurally disordered on the silica (0001) surface, leading to a remarkable enhancement of the Li-ion conductivity (6×10^{-6} S cm^{-1} at 50 °C, with an activation energy of 0.55 eV) of three orders of magnitude. The resulting conductivity is not exceedingly high, but is comparable with that of the current, best thin-film solid electrolyte ($Li_{(3+x)}PO_{(4-x)}N_x$). The conductivity is highest if a significant density of glass/ceramic interfaces is achieved and percolation of the interfaces guaranteed.

1. Introduction

While liquid or semi-liquid electrolytes that can penetrate nanostructured electrode materials are preferred for high-performance batteries, Li-conducting thin-film electrolytes are the candidate of choice for the integration of micro-power-sources into microdevices.[1–3] In past years, the progress of developing novel solid electrolytes has focused mainly on the exploration of new crystalline or amorphous materials and their conditioning by doping.[4–7]

One of the promising modern strategies to develop better solid electrolytes is the generation of heterogeneous systems instead of the above-mentioned homogenous ones. Even though the discovery of composite LiI/Al_2O_3 electrolytes with a conductivity enhancement close to two orders of magnitude as compared with pure LiI by Liang in 1973[8] triggered the development of a huge number of new heterogeneous electrolytes,[9] heterogeneous systems composed of Li-ion conductors (e.g., LiX•xH$_2$O, X = I, Br and Li_3PO_4) are, nonetheless, rather rare.[10–15] Here we report on conductivity effects in LiF films on SiO_2 substrates, which we correlate with the presence of glass-crystal interfaces. Adams et al.[16] showed the beneficial influence of glass/ceramic interfaces in Ag-conducting systems. More recently, Schirmeisen et al.[17] verified the existence of a fast ion conduction interfacial regime between the glassy and crystalline phases.

LiF is intrinsically of poor conductivity compared with other lithium halides and is usually well crystallized in contact with a substrate.[18–20] These properties make it a good prototype material in terms of exploring space-charge effects, and much room is left for the adjustment of the charge carrier concentration. In this respect, we could interpret results of LiF films on Al_2O_3 and TiO_2 substrates.[21,22] Very unexpectedly, we found a different behavior for SiO_2 substrates, in that the LiF thin films become seriously structure-disordered when in contact with the SiO_2 surface. The observed conductivity enhancement is greater than what we would expect for ion-accumulation space-charge effects. Our LiF films exhibit various degrees of crystallinity that can be varied by two control parameters: one is the temperature, the other is the film thickness.

2. Results and Discussion

X-ray diffraction (XRD) patterns of LiF thin films with various thicknesses and annealing temperatures on SiO_2 (0001) substrates are shown in **Figure 1**a. The (111) and (200) diffraction peaks are thickness dependent, developing from sheer absence to the growth of these diffraction signals with a thickening of the films. In addition, the peaks, that were originally weak and wide, become increasingly distinguishable with increasing temperature. This indicates that as-fabricated and moderately annealed thin films were present in polycrystalline form, but were structurally disordered to a high degree. The transmission electron microscopy (TEM) image is focused on the cross-section of a 250 nm-thick LiF sample, annealed at 300 °C (Figure 1b). It clearly reveals that the bulk phase of the thin film was not homogeneous, and, therein, numerous dark spots were densely embedded in the light-colored medium. Using high-resolution TEM (HR-TEM), we further discovered that the small spots could be ascribed to nanograins of well-crystallized LiF that were embedded in the amorphous LiF (Figure 1c). A region about 2 nm thick could be detected, forming the transition from the crystalline to the glassy phase (Figure 1d). Otherwise, the interface between the LiF thin film and the SiO_2 substrate was well defined, indicating the absence of serious mass inter-diffusion and high-fraction interfacial phases.

Dr. C. L. Li, Prof. J. Maier
Max Planck Institute for Solid-State Research
Heisenbergstraße 1, D-70569 Stuttgart, Germany
E-mail: C.Li@fkf.mpg.de
Prof. L. Gu
Institute of Physics
Chinese Academy of Sciences
Beijing 100190, China

DOI: 10.1002/adfm.201101798

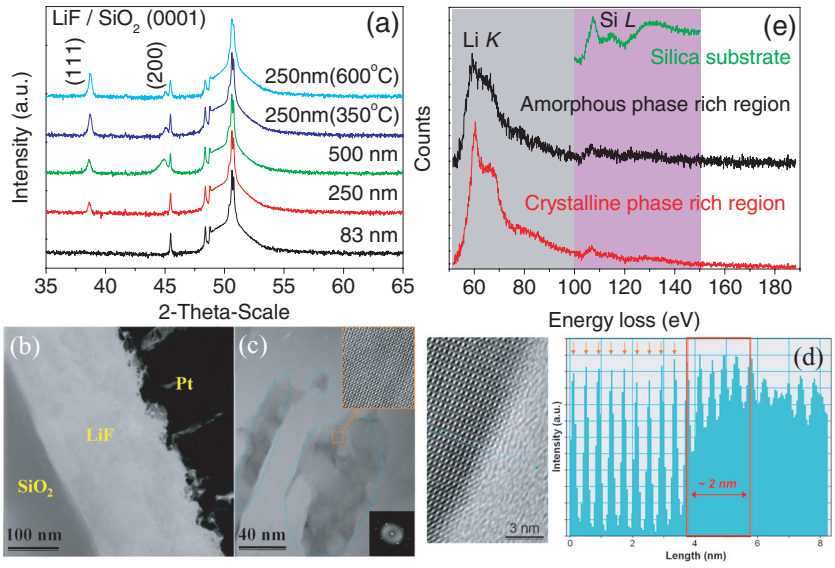

Figure 1. a) XRD patterns of as-deposited LiF thin films of various thicknesses on SiO_2 (0001) substrates, as well as under different annealing treatments, for 250 nm thick films. b) Cross-section TEM image of LiF bulk phase and LiF-SiO_2 interface for the 300 °C annealed thin film. c) HR-TEM image of the enlarged LiF bulk phase of the heterogeneous structure, where well-crystallized nanograins (dark) are imbedded in an amorphous matrix (light-colored). Inset: Crystal lattice stripes of the designated dark region. d) Line profile of structure information through the amorphous-crystalline interface. e) EELS of Li *K* and Si *L* edges in amorphous- or crystalline-phase-rich region, with that of a pure-SiO_2 substrate as a comparison.

It should be noted that LiF thin films are prone to being highly textured along certain crystalline orientations on a great number of substrates, including amorphous ones, even under room-temperature deposition.[18–20,23] Therefore, it is much more likely that the amorphization of the original cubic LiF did not result from a lattice mismatch with the (0001) plane of the SiO_2 single crystals, but rather from the facile migration of SiO_2 into the thin film during plasma bombardment on the substrate, or the chemical incorporation of LiF into the nucleation sites of the SiO_2 surface during the initial deposition.[24] Indeed, Si (Si *L*) could be detected in electron energy-loss spectroscopy (EELS) of the thin films (Figure 1e), and its atomic percentage in the amorphous-rich regions (≈15%) was almost twice as high as in the crystalline-rich regions (≈8%). This also agrees with the much-more-defined profile of the Li *K* edge in the crystalline-rich region. Combined with the poorly defined Si *L* profile in the thin films and the detectable traces of oxygen (see EELS in Figure S1, Supporting Information), it was concluded that the amorphization of LiF was caused by an admixture of silica serving as a glass-network former. This would explain the thickness dependence of the degree of amorphization directly. If the Si were introduced during substrate conditioning, it is very conceivable that the silica would be diluted when the film thickness is increased, leading to the formation of larger LiF crystal grains (provided the deposition time is long enough) as indicated by the XRD results (also see the scheme in **Figure 2**). Assuming the first nucleation of LiF atoms to be fast enough, a continuous layer, rather than isolated islands, would be expected to form, followed by successive layer-type growth, in agreement with the observed thin-film morphology free of voids.

The degree of amorphization could also be decreased and the crystal size increased by increasing the preparation temperature. **Figure 3**a and 3b show how significantly the thin-film microstructure evolution, depending on the equilibrium temperature, influences the electrical behavior. They display typical Nyquist plots of 125 nm-thick LiF thin films equilibrated at 350 °C and 600 °C, respectively. At the same testing temperature (350 °C), both show complete semicircles, which can be well fitted by a corresponding equivalent circuit made up of three parallel components (i.e., stray capacitance, C_{stray}, bulk capacitance, C_{bulk} and total resistance, R_{total}). C_{stray} is associated with the well-defined sample geometry and is on the order of 10^{-12} F. Assuming that the relative dielectric constant (ε) of LiF is in the range of 10–100 for the conditions under

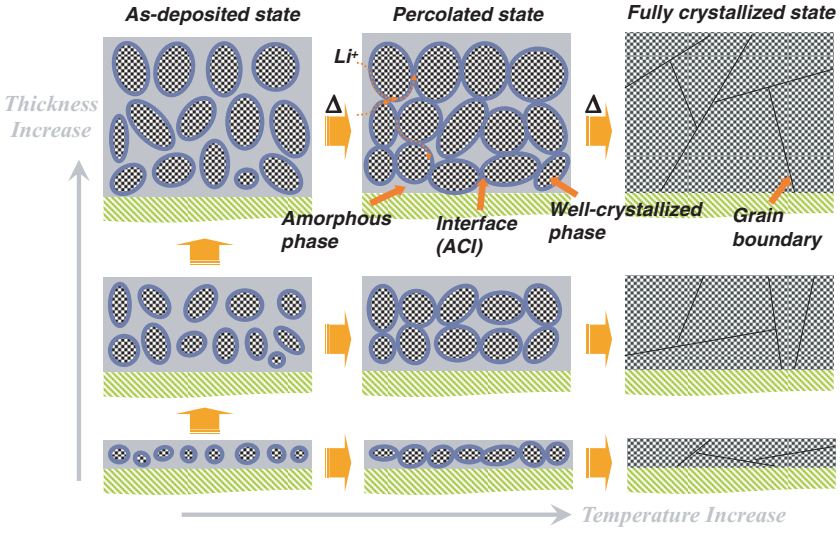

Figure 2. Scheme of the microstructure and morphology of the as-deposited LiF thin films, depending on different thicknesses, as well as their crystallization process at various annealing temperatures. As-deposited state: the LiF grain crystals embedded in the amorphous matrix in the cross-section of the bulk phase grow with the increase of deposition time. The interconnected amorphous region serves as the dominant ion-conduction path. Percolated state: the percolating interface between the amorphous and the well-crystallized LiF phases (ACI) serves as the dominant conduction path at a certain crystallization stage. Fully crystallized state: under further annealing at the higher temperatures, the ACIs evolve into grain boundaries, along with the shrinkage of the amorphous phases. The crystallographic sites of cubic LiF, as well as the grain boundaries, serve as the Li-ion migration channels.

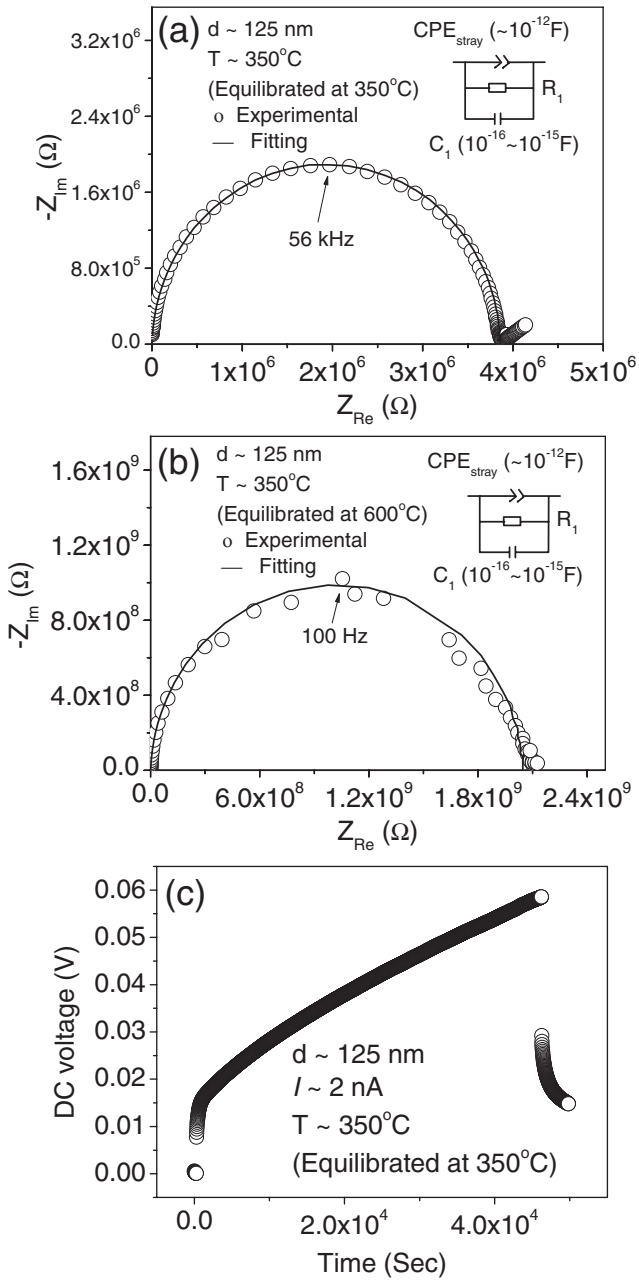

Figure 3. a,b) Nyquist plots of LiF thin films equilibrated at 350 °C (a) and 600 °C (b). Insets: equivalent circuit for fitting the experimental data. c) DC polarization curve of LiF thin film equilibrated at 350 °C. The film thickness was 125 nm and the testing temperature was 350 °C.

concern,[25] C_{bulk} was calculated to be in the range 10^{-16}–10^{-15} F (although an ε value close to 100 is extremely high, it has indeed been measured for LiF after polarization or irradiation[25]). It can also not be excluded that the disordered LiF thin films measured at high temperature had a different ε value to that of perfect LiF crystals. In all cases, however, the stray capacitance should dominate the high frequency. The sample equilibrated at 350 °C was characterized by an obvious diffusion tail at low frequencies, and had a much-smaller R_{total} by almost three orders of magnitude than that equilibrated at 600 °C. The ion conductivity of ≈2×10^{-3} S cm^{-1} at 350 °C is 2–3 orders of magnitude higher than the single-crystal or the well crystallized thin-film values.[21,22,26,27] The direct-current (DC) polarization curve for the former, using ion-blocking Pt electrodes (Figure 3c), is quite sloped and confirms the dominant ion conductivity (mainly lithium vacancy V'_{Li}[28]).

Figure 4 shows parallel-conductivity ($\sigma^{\parallel}$) plots of the LiF thin films for various thicknesses and heating-stabilization-cooling cycles. By heating the as-deposited samples from room temperature up to 600 °C, three distinct stages of conductivity development are observed (Figure 4a). At the beginning, the conductivity increases on heating in a quasi-Arrhenius behavior. Then, at about 350 °C, a conductivity drop occurs. With the follow-up heating up to 600 °C, the conductivity increases once more in a similar manner to that observed initially. This qualitative feature was independent of film thickness (Figure S2, Supporting Information). When the heating process was terminated and then stabilized at 350 °C, the conductivity plots during the following cooling obeyed an accurate Arrhenius behavior. The situation was also similar after thermal equilibration at 600 °C. Interestingly, both the conductivity and the activation energy (E_a) depend greatly on the equilibration temperatures, as shown in the corresponding Nyquist plots (Figure 3a and 3b). This behavior is similar to that observed by Adams et al.[16]

The poorly defined LiF diffraction peaks in the as-fabricated samples are likely to have been caused by the existence of a high proportion of amorphous phase (including a significant density of defective transition zones). Owing to the low conductivity of Li ions in the LiF crystal structure for the as-fabricated or moderately annealed samples, Li-ions were likely to move mainly through the interconnected amorphous matrix rather than the crystalline phase. The thermally controlled growth of the LiF crystal grains, indicated by the much more discernable diffraction peaks of the sample annealed at 350 °C, leads to a shrinkage of the amorphous region. The thus-increased portion of the interface zones between the amorphous and crystalline phases (ACI), as defined in the HR-TEM results shown in Figure 1d, leads to a greater percolation probability for the interfacial transport. The nature of ACIs was not expected to greatly change in view of the epitaxial crystallization at interfaces.[29] When the samples were equilibrated at 350 °C, the slope of the profiles of conductivity plots became much lower, compared with other heating stages. We observed quite high $\sigma^{\parallel}$ and low E_a values (e.g., $\sigma^{\parallel} \approx 6 \times 10^{-6}$ S cm^{-1} (50 °C) with an E_a of 0.55 eV for the 250 nm-thick sample (Figure 4b)), suggesting that the Li ions mainly migrate along the network of the percolating ACIs. HR-TEM revealed that the crystallites were typically separated by a disordered layer, allowing the amorphous phase as well as the ACIs to percolate (Figure S3, Supporting Information). In contrast, the conductivity performance degraded by almost three orders of magnitude, with a much larger E_a of ≈0.98 eV after equilibration at 600 °C (Figure 4c), consistent with the transport properties of LiF single crystals, as well as with the bulk behavior of LiF thin films.[21,26,27] This should be ascribed to the interruption of the ACI due to further crystallization (i.e., to the formation of crystal/crystal contacts at the cost of the ACI), eventually leading to the disappearance of the amorphous regions. During crystallization, the doped SiO_2 in

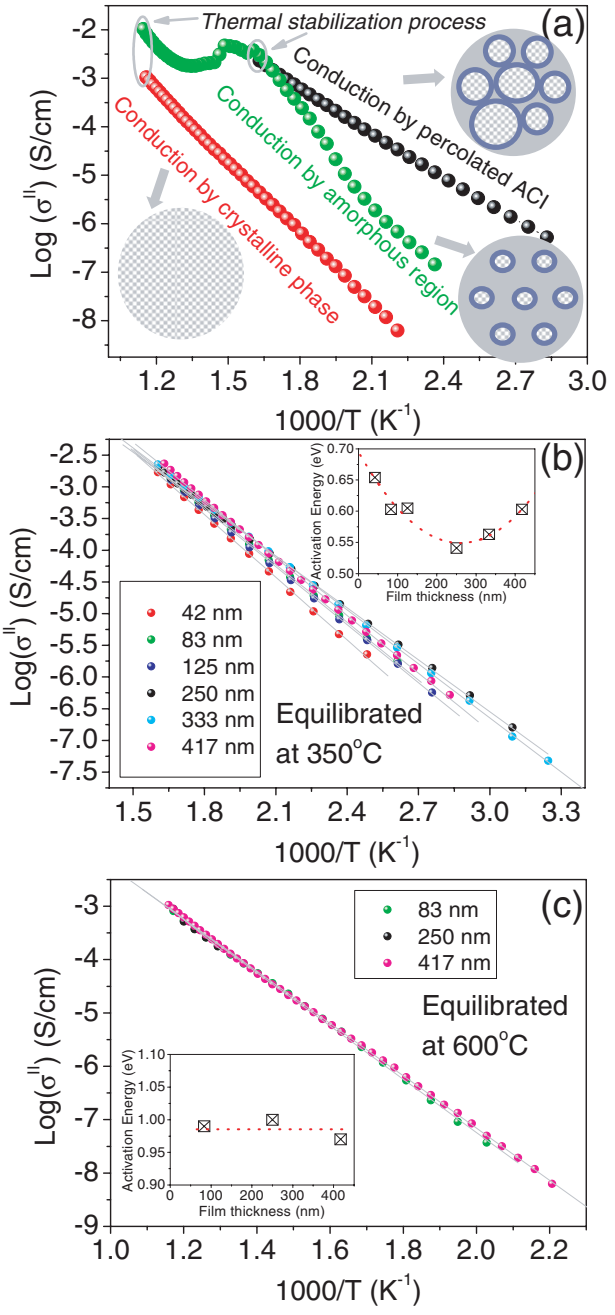

Figure 4. a) Arrhenius plots of LiF thin films (417 nm) during different heating-stabilization-cooling cycles with corresponding Li^+-migration paths. By heating from room temperature up to 600 °C (green plots), the conductivity increases initially in a Arrhenius-type behavior, then deviates from it in the direction of higher values, reaches a maximum after which it degrades, and finally increases once more in an Arrhenius manner. When the heating process is interrupted at 350 °C (black plots) or 600 °C (red plots), the conductivity obeys accurate Arrhenius behavior during the following cooling (high conductivity before degradation and poor conductivity of the crystalline phase after degradation). Insets: Sketches of the microstructure development due to the growth of LiF crystal grains at the various stages. b,c) Arrhenius plots of LiF thin films of various thicknesses during the cooling process with a prior thermal equilibrium at 350 °C (b) and 600 °C (c). Insets: Thin-film thickness dependence of the activation energy under corresponding equilibrium conditions.

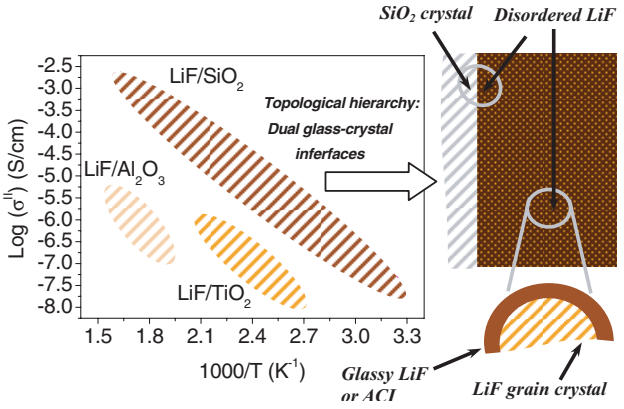

Figure 5. Arrhenius plot regions of LiF-SiO_2, LiF-TiO_2 and LiF-Al_2O_3 systems, in view of a comparison of the microstructure effect with ionic space-charge accumulation/depletion effects. Right: Scheme of topological hierarchy characterized by dual glass-crystal interfaces in the LiF-SiO_2 system.

the glassy phases is expected to be squeezed into grain boundaries or triple junctions of the fully crystallized phase (Figure 2).

Thus, three Li^+-migration paths can be found in the films with distinctly different local conductivities ($\sigma_{ACI} > \sigma_{glass\ phase} > \sigma_{crystal\ phase}$), agreeing well with previous measurements by time-domain electrostatic force spectroscopy of a nanostructured $LiAlSiO_4$ glass ceramic,[17] as well as with the behavior of Ag-conducting glass-ceramics.[16] The formation of interfacial phases between the LiF and the SiO_2 can be ruled out from the TEM results. Also, the Arrhenius plots of the different thin-film thicknesses overlap after 600 °C equilibrium, as shown in Figure 4c, which could not be brought into consistency with interfacial effects at the LiF/SiO_2 contacts. In contrast, it was found that the E_a after 350 °C equilibrium was in the range of 0.55–0.65 eV, slightly depending on the thickness, with a minimum located at a moderate thickness of 250 nm (inset of Figure 4b). The parabolic thickness dependence of the E_a should be associated with the density and interconnection topology of the ACI network.

Figure 5 shows a comparison of the conductivity values induced by microstructural effects with those obtained by space-charge effects of LiF thin films on other substrates. Preferential ion absorption (Li^+ at TiO_2) or adsorption (F^- at Al_2O_3) at a given contact leads to an accumulation or a depletion of the V'_{Li} concentration close to the interface.[21,22] However, a conductivity enhancement by one order of magnitude, observed from the carrier accumulation (e.g., from the order of 10^{-7} to 10^{-6} S cm^{-1} at 225 °C), does not bring the LiF into a conductivity range that makes it interesting as a solid electrolyte. The present effect though, which is still not optimized, offers distinctly higher values, already on the level of the most popular thin-film electrolyte $Li_{(3+x)}PO_{(4-x)}N_x$.[1,2]

The fact that, after preparation, the final transport properties do not rely on the presence of the SiO_2 substrate makes it even more interesting for possible applications. From the fundamental point of view, the key question is about the origin of the enhancement. From a crystal point of view, it is tempting to relate the transition zone to the high density of dislocations (as observed in the HR-TEM in Figure 1d), which have been shown to display a similar behavior in various composite elec-

trolytes.[30–34] In these systems, they seem to be notoriously charged and can be thermally healed out. Indeed the activation energy (see Figure 4b) is not far from the migration energy of lithium vacancies (≈0.65–0.75 eV[35,36]), which would be expected from a space-charge point of view. Nevertheless, one would expect it to be slightly lower, rather than slightly higher, and also the effect of the transition zone seems to be thermally more stable in our case. On the other hand, we refer to an amorphous phase and we expect the crystal-based pictures to be blurred with respect to influences by local-structure, migration-energy and space-charge effects. Hence, we expect a greater structural inhomogeneity and a lower charge separation. More experiments, however, are necessary to shed light on this exciting structural regime.

3. Experimental Section

The LiF thin films were grown by radio-frequency (RF) sputtering with an RF power of 30 W on acetone-cleaned single-crystal-silica (0001) substrates at room temperature. The ambient pressure was kept at 10^{-2} mbar through a pure-argon inflow. The growth rate was controlled to be at about 3 nm min^{-1} and the film thickness was in the range of 40–500 nm. XRD and TEM (where the lamellae for the film cross-section were cut by a focused ion beam (FIB)) were used to analyze both the microstructure and the morphology, as well as the film thickness. EELS was performed to detect the element distribution, especially possible component diffusion from the substrate to the bulk phase of the thin films. To measure the in-plane conductivity, two rectangular Pt electrodes, with a thickness of 400 nm and a length of 10 mm, were deposited with a 1 mm spacing on the sample surfaces by DC sputtering at room temperature. Conductivities during different heating/cooling cycles (from room temperature to 600 °C) were measured by alternating-current impedance spectroscopy, with a frequency ranging from 2 MHz to 1 Hz, in an argon atmosphere. The time interval between two adjacent conductivity plots was 2 h. Prior to each cooling process, the samples were stabilized at different equilibration temperatures for 20 h. DC-polarization measurements were also performed with Pt electrodes to estimate the contribution of ionic conduction. The conductivity contribution from bare silica substrates could be neglected.

Supporting Information

Supporting Information is available from the Wiley Online Library or from the author.

Acknowledgements

The authors thank G. Götz and B. Fenk for the XRD measurements and the TEM lamella preparation by FIB of the LiF thin-film samples. The authors also thank Dr. F. Phillipp, K. Hahn, and X. K. Mu for their help in the EELS measurements.

Received: August 3, 2011
Revised: November 14, 2011
Published online: January 23, 2012

[1] X. H. Yu, J. B. Bates, G. E. Jellison, F. X. Hart, *J. Electrochem. Soc.* **1997**, *144*, 524.
[2] C. L. Li, Z. W. Fu, *J. Electrochem. Soc.* **2007**, *154*, A784.
[3] C. L. Li, B. Zhang, Z. W. Fu, *Thin Solid Films* **2006**, *515*, 1886.
[4] Y. Inaguma, L. Q. Chen, M. Itoh, T. Nakamura, T. Uchida, H. Ikuta, M. Wakihara, *Solid State Commun.* **1993**, *86*, 689.
[5] R. Murugan, V. Thangadurai, W. Weppner, *Angew. Chem. Int. Ed.* **2007**, *46*, 7778.
[6] R. Kanno, M. Murayama, *J. Electrochem. Soc.* **2001**, *148*, A742.
[7] A. Hayashi, S. Hama, T. Minami, M. Tatsumisago, *Electrochem. Commun.* **2003**, *5*, 111.
[8] C. C. Liang, *J. Electrochem. Soc.* **1973**, *120*, 1289.
[9] J. Maier, *Prog. Solid State Chem.* **1995**, *23*, 171.
[10] J. B. Phipps, D. H. Whitmore, *Solid State Ionics* **1983**, *9–10*, 123.
[11] B. Wassermann, T. P. Martin, J. Maier, *Solid State Ionics* **1988**, *28–30*, 1514.
[12] D. Lubben, F. A. Modine, *J. Appl. Phys.* **1996**, *80*, 5150.
[13] H. Maekawa, R. Tanaka, T. Sato, Y. Fujimaki, T. Yamamura, *Solid State Ionics* **2004**, *175*, 281.
[14] A. C. Khandkar, J. B. Wagner, *Solid State Ionics* **1986**, *20*, 267.
[15] M. Nagai, T. Nishino, *Solid State Ionics* **1994**, *70–71*, 96.
[16] S. Adams, K. Hariharan, J. Maier, *Solid State Ionics* **1995**, *75*, 193.
[17] A. Schirmeisen, A. Taskiran, H. Fuchs, H. Bracht, S. Murugavel, B. Roling, *Phys. Rev. Lett.* **2007**, *98*, 225901.
[18] W. S. Tsang, C. L. Mak, K. H. Wong, *Appl. Phys.* **2003**, *A 77*, 693.
[19] G. Baldacchini, M. Cremona, S. Martelli, R. M. Montereali, L. C. S. Docarmo, *Phys. Status Solidi. A* **1995**, *151*, 319.
[20] X. Q. Yu, J. P. Sun, K. Tang, H. Li, X. J. Huang, L. Dupont, J. Maier, *Phys. Chem. Chem. Phys.* **2009**, *11*, 9497.
[21] C. L. Li, X. X. Guo, L. Gu, D. Samuelis, J. Maier, *Adv. Funct. Mater.* **2011**, *21*, 2901.
[22] C. L. Li, L. Gu, X. X. Guo, D. Samuelis, K. Tang, J. Maier, unpublished.
[23] A. Perea, J. Gonzalo, C. N. Afonso, S. Martelli, R. M. Montereali, *Appl. Surf. Sci.* **1999**, *138–139*, 533.
[24] M. Kislitsyn, S. M. Haile, *Chem. Mater.* **2010**, *22*, 2417.
[25] N. Veeraiah, *J. Mater. Sci.* **1987**, *22*, 2017.
[26] T. G. Stoebe, *J. Phys. Chem. Solids* **1967**, *28*, 1375.
[27] G. Geschwind, *J. Phys. Chem. Solids* **1969**, *30*, 1631.
[28] T. G. Stoebe, R. A. Huggins, *J. Mater. Sci.* **1966**, *1*, 117.
[29] I. T. Bae, Y. W. Zhang, W. J. Weber, M. Higuchi, L. A. Giannuzzi, *Appl. Phys. Lett.* **2007**, *90*, 021912.
[30] X. X. Guo, I. Matei, N. Y. Jin-Phillipp, P. A. van Aken, J Maier, *J. Appl. Phys.* **2009**, *105*, 114321.
[31] J. Fleig, F. Noll, J. Maier, *Ber. Bunsenges. Phys. Chem.* **1996**, *100*, 607.
[32] J. D. Eshelby, C. W. A. Newey, P. L. Pratt, A. B. Lidiard, *Philos. Mag.* **1958**, *3*, 75.
[33] R. A. De Souza, J. Fleig, J. Maier, Z. L. Zhang, W. Sigle, M. Rühle, *J. Appl. Phys.* **2005**, *97*, 053502.
[34] J. Maier, *Physical Chemistry of Ionic Materials: Ions and Electrons in Solids*, Wiley, Chichester **2004**.
[35] Y. Haven, *Recl. Trav. Chim. Pays-Bas* **1950**, *69*, 1471.
[36] K. Alexopoulos, M. Lazaridou, P. Varotsos, *Phys. Rev. B: Condens. Matter* **1986**, *33*, 2838.